UNIVERSITY OF CALIFORNIA, SAN DIEGO

Ultrastructure Alterations in Pathological Fibrotic Skeletal Muscle of Mice and Humans

A thesis submitted in partial satisfaction

of the requirements for the degree Master of Science

in

Biology

by

Rachel Carolyn Meza

Committee in charge:

Professor Richard Lieber, Chair
Professor William Kristan, Co-Chair
Professor Kathleen French

2015

The Thesis of Rachel Carolyn Meza is approved, and it is acceptable in quality and form for publication on microfilm and electronically:

Co-Chair

Chair

University of California, San Diego

2015

DEDICATION

I would like to dedicate this thesis to my parents. Thanks to their constant support, care, generosity and humor, I grew up with the two most amazing role models any child could ask for. Nothing was out of reach with these two loving individuals by my side. I always knew I was destined to go to graduate school. Rest assured, one step down, one more step to go! I guess, what I'm trying to say is that I love you both!

EPIGRAPH

You are always a student, never a master. You must **keep moving forward**

Conrad Hall

TABLE OF CONTENTS

SIGNATURE PAGE iii

DEDICATION iv

EPIGRAPH v

TABLE OF CONTENTS vi

LIST OF ABBREVIATIONS vii

LIST OF TABLES viii

LIST OF FIGURES ix

LIST OF SUPPLEMENTAL FILES x

ACKNOWLEDGEMENTS xi

ABSTRACT OF THE THESIS xii

I. Introduction 1

II. Materials and Methods 9

III. Results 16

IV. Discussion 33

REFERENCES 39

SUPPLEMENTAL FILES 42

LIST OF ABBREVIATIONS

Cerebral Palsy ……. CP

Extracellular Matrix …… ECM

Gross Motor Function Classification Score ……... GMFCS

Nesprin/Desmin Double Knock-out mice ……... DKO

Serial Block Face Scanning Electron Microscopy ……... SBFSEM

Scanning Electron Microscopy …… SEM

Tibialis Anterior ……. TA

Transmission Electron Microscopy ……. TEM

Typically Developing ……. TD

LIST OF TABLES

Table 1: Patient Considerations 17

Table 2: Murine Considerations..... 17

LIST OF FIGURES

Figure 1: Muscular Anatomy. 3

Figure 2: Collagen isoform concentrations are increased proportionally in CP.. 19

Figure 3: Developing a new immersion fixation protocol. 22

Figure 4: Comparisons of wild-type and double knockout mice. 25

Figure 5: Comparisons of typically developing and cerebral palsy patients 28

Figure 6: A change in myofibril orientation within myofibers. 30

Figure 7: Correlating of areas of interest found in TEM to X-ray to SEM 32

LIST OF SUPPLEMENTAL FILES

Supplemental Figure 1: Group 1 – wildtype and double knockout mice 42

Supplemental Figure 2: Group 2 – double knockout mouse..... 43

Supplemental Figure 3: Typically developing patient..... 44

Supplemental Figure 4: Cerebral palsy patient 1..... 45

Supplemental Figure 5: Cerebral palsy patient 2..... 46

Supplemental Figure 6: Cerebral palsy patient 3..... 47

ACKNOWLEDGEMENTS

I would first like to express my appreciation to Dr. Rick Lieber for giving me the opportunity to work in his lab not only as an undergraduate volunteer, but also for letting me continue my passion for the project as a graduate student. He has been a key player in shaping me as a researcher, showing me how to look at problems and interpret answers. I also thank my committee members Dr. Kristan and Dr. French for their time and effort.

I would also like to thank all the members of the Lieber, Ward, Shah, and Schenk lab for their mentoring and support. Particularly I'd like to thank Rajeswari Pichika for taking me under her wing as an undergraduate. She is kind and patient, the two best qualities for a mentor to have. I'd like to extend a special thank you to Margie Mathewson, Mark Chapman, and Kevin Young for showing me that graduate school can indeed be a fun place as long as you have the right people by your side. Their continual counsel and laughter helped make the long days worthwhile. Additionally, I thank Rajewswari for her contribution to Figure 1, and to Mark for the use of his mice.

Lastly, I would like to express my gratitude to the Ellisman lab. Foremost, I thank Dr. Mark Ellisman for allowing me the opportunity to work with such cutting-edge technology. I would especially like to thank Eric Bushong, Tom Deernick, Mason Mackey, Andrea Thor and Christine Kim, who went above and beyond in training me on the microscopes and helping me with my questions. Without their generosity in their time, this project would not have been completed.

Certainly not unforgotten, I would like to thank all my family and friends for their encouragement and support throughout the years.

ABSTRACT OF THE THESIS

Ultrastructure Alterations in Pathological Fibrotic Skeletal Muscle of Mice and Humans

by

Rachel Carolyn Meza

Master of Science in Biology

University of California, San Diego, 2015

Professor Richard Lieber, Chair

Professor William Kristan, Co-Chair

It is considered that excessive extracellular matrix (ECM) content, specifically an increase in collagen concentration, may be causing the disruption of normal muscle mechanics in disorders presenting muscular stiffness. A clinical example is cerebral palsy (CP), caused by a neurological pathology, that results in muscle spasticity, uncontrolled movements, and/or contractures. An example of excess ECM is also known as skeletal muscle fibrosis. Thus we used both cerebral palsy muscles and fibrotic mouse muscles as

our models for muscle stiffness. Our aim was to elucidate the collagen environment in stiff muscles compared to control muscles, in order to find a functional relationship to stiffness. Collagen content was quantified via ELISA and was found that all of the four main stiffness collagen isoforms have a 2.46 ± 0.19 fold increase in CP. However, these increases are at ratios proportional to concentrations found in control. Further investigations on the structure of collagen tendrils in a fibrotic environment are currently underway utilizing a new imaging technique referred to as Serial Block Face Scanning Electron Microscopy (SBFSEM), which gives a 3D reconstruction of the ultrastructure. Preliminary data is showing a trend towards an increase in fibroblasts as the cause of the collagen increase in the fibrotic mouse model. More human model samples will have to be tested for further conclusions on collagen packing and fibroblast number. Bearing in mind that muscle function is highly correlated with the ECM network, these findings may suggest that increased stiffness in fibrosis could be due to irregular ECM remodeling.

I:

Introduction

Skeletal Muscle Anatomy and Physiology

There is a strong structure-function relationship in muscles and their environment. Muscles span two joints and are connected to the bones by tendons. When a muscle receives a signal to contract, sarcomere components slide past each other, which pull on the tendons and produce a force that we call movement. Muscles are divided into fascicles and connective tissue (Figure 1). Nestled underneath the basal laminal covering of the myofiber, but above the sarcolemma, is the niche for satellite cells, or muscle progenitor cells. These satellite cells are responsible for all post-natal myofiber growth and repair. Delving further underneath the sarcolemma are the contractile components, collectively called myofibrils. Myofibrils are serial chains of sarcomeres, composed of actin (thin) filaments and myosin (thick) filaments, which are the core components of contraction in the muscle. These two filaments, along with the sarcoplasmic reticulum and the muscles' intracellular concentrations of Ca^{2+} and ATP, form the excitation-contraction coupling system. Described above are the active components of muscles. There are also the passive components, provided by the extracellular matrix (ECM). Extracellular matrix serves as a structural support as well as force transduction; and as such is an important component in muscle functionality and adaptability.

With a change in passive mechanics, such as in a diseased condition, muscles can become very stiff. However, it is still unanswered as to what causes muscle stiffness. Our lab sought to answer this question by focusing on the lesser known passive properties, by finding alterations in the extracellular matrix; an often undervalued but highly important component to muscle function. We did so by using looking into the ultrastructure of both animal and human models of fibrosis.

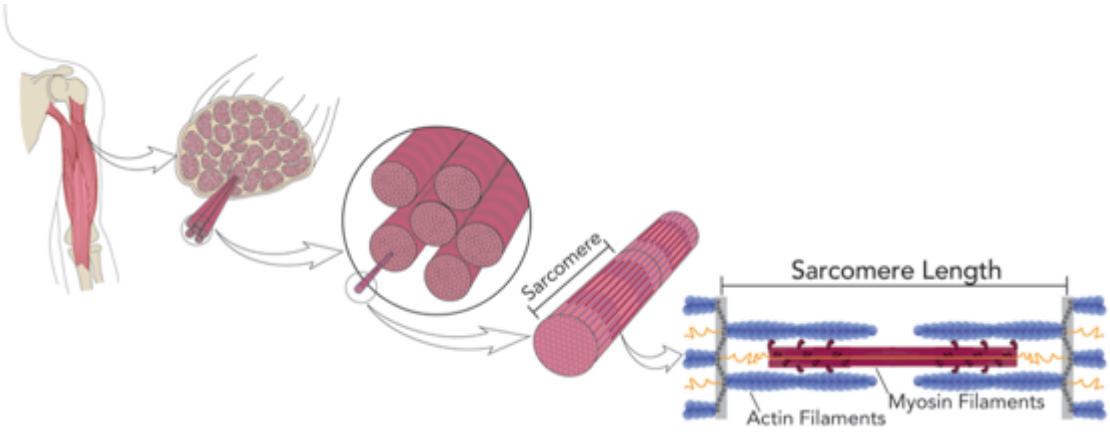

Figure 1: Muscular Anatomy. The figure above depicts the hierarchical levels of the muscle, starting from the left at the whole muscle structure, which is surrounded by the layer of connective tissue known as the epimysium. Delving inside are muscle fascicles, which are bundles of myofibers surrounded by the perimysium. Each bundle is comprised of many myofibrils or sarcomere chains and the endomysium. Sarcomeres are the basic building blocks of muscle and the source of force production in muscles via actin and myosin filaments. Figure modified from Lieber Skeletal muscle structure and function.

Skeletal Muscle Stiffness, Extracellular Matrix, and Fibrosis

Previous data has not been able to functionally correlate the passive mechanics in many stiff diseased models to any known component. A well-known clinical example of a diseased stiff muscle is cerebral palsy (described more in detail in a later section). Initial attempts in cerebral palsy muscles found that the intramuscular component titin, the typical indicator of stiffness, (Prado et al., 2005) was unaltered (Smith et al. 2011). New insights point to the extracellular matrix (ECM) for causing the disruption of normal muscle function (Lieber et al. 2003; Meyer et al. 2011) The ECM provides most of the strength and passive compliance of the muscle through its components collagen, fibronectin, proteoglycans and other non-collagen proteins. ECM is divided into endomysium, perimysium and epimysium, division based mostly on morphology. The differences in components of the three types of ECM are rare; almost all ECM is composed of the same structural and biochemical components (Gillies et al., 2011).

Collagen is the basic structural support of connective tissue, and it is because of this support that collagen is likely the extracellular element that plays a role in load-bearing properties, as determined by its network arrangement. In the proper concentrations, collagen acts as a scaffold for typical development, injury repair, and normal muscle tissue maintenance. Extreme amounts, such as in fibrosis, can result in serious effects on mobility, by limiting the space and tension that can be produced by muscle fibers. Fibrosis can be defined in a number of ways, depending on the tissue in question. For the purposes of this research, skeletal muscle fibrosis is designated as an excessive accrual of extracellular matrix. This is usually due to chronic inflammation, in which fibrotic tissue is replacing the muscle, however this is not always the case. (Mann et al., 2011). Fibrosis can lead to successive muscular atrophy. Understanding fibrosis in multiple models allows for specified treatments in each disorder where fibrosis is present.

A few studies have begun to look at ECM content in stiff muscles, specifically talked about here is cerebral palsy. It was found that patients with CP had an increase in muscle collagen, correlating with an increase in severity in spasticity (Booth et al., 2001). Booth indicated that this finding suggests that the collagen accumulation is forming contractures and possibly restricting growth of the muscle. Similarly, Smith (2011) and Lieber (2003) also showed an increase in collagen deposition and an alteration in the passive mechanics of the muscle. However, these fibrosis and stiffness have not been correlated as causation as of yet.

Thus, total collagen content may not tell the whole story. Quantifying the type of collagen could bring insights as well. Collagen has over 25 known isoforms, comprising of both fibrillar isoforms and laminar isoforms. Type I is by far the most common

isoform (which happens to be fibrillar) and is associated with high tissue stiffness, or the resistance to stretch (Gelse, 2003). Type III is the next most common fibrillar and associated with high tissue compliance (Miller et al., 2001; von der Mark, 1981). Type IV is the most common laminar and Type VI is still undergoing research but is associated with satellite cell regeneration (Urciuolo et al., 2013). All isoforms have the same basic triple helix structure, made of three chains (denoted as α-chains). The chains vary in sequence and length, all with the characteristic Glycine-Proline-Hydroxyproline sequence, contributing to different functions for each isoform. Type I, for example, has two α-1 helices and one α-2 helix whereas Type III has three α-1 helices but each provides a different mechanical purpose, as described above. Collagen assembles into fibers in a staggered, striated pattern, clearly visible under the microscope. The similarity in structure between these two isoforms leads to some cross-reactivity in antibodies specific for each type. Knowing this fact ahead of time allows for compensation.

Nesprin-Desmin Double Knockout Mice – An Animal Model of Fibrosis

To understand fibrosis on a larger level, we employed the use of a fibrotic animal model, a nesprin/desmin double knockout mice (Chapman et al., 2014). In these mice, the survival curve was much steeper, balance and grip strength were reduced and force production was diminished. Studies also showed an increase in total collagen content and an increase in muscle stiffness. The benefit of using these mice is that we could compare known fibrotic biochemical pathways to the fibrosis we expect to observe.

Cerebral Palsy – A Human Model of Fibrosis

Cerebral Palsy (CP) is defined as group of disorders affecting body movement, balance, and posture, among other things. Cerebral Palsy is one of the most common

congenital disorders in the United States, with approximately 2 in 1,000 children diagnosed in the United States (Ken Stern, 1997). It is caused by abnormal development or damage to the motor cortex of the developing brain, and results in muscle stiffness (spasticity), poor muscle tone, and uncontrolled voluntary movements (ataxia). Spastic muscles are defined as having hyper-reflexia and increased muscle response (Crenna, 1998); and have a tendency to develop into contractures, in which a muscle becomes painfully stiff due to chronic activation of the fibers. Symptoms begin to appear within the first three years of a child's life. Unfortunately, there is no cure for this disorder, as it is neurological and currently irreversible. However, there are surgical treatments that can temporarily alleviate stiffness or postpone pain, along with physical therapy. Improvements on these treatments are currently being researched to help patients with cerebral palsy deal with the associated muscular disorder.

There is a range of disabilities associated with cerebral palsy; as such, there is a wide range of classification systems in use today, all of which are constantly being updated as research brings in more knowledge about the condition. The easiest way to consider the condition is to break it down into a hierarchy, based on both motor function capabilities and location of brain injury. First, a patient is described as spastic or non-spastic, with spasticity accounting for the majority of the cases. They are also referred to as pyramidal, as the brain injury occurs on the pyramidal tract (or upper motor cortex) and extrapyramidal respectively. Spastic conditions can be divided into three more categories, depending on the topological degree of impairment. In a hemiplegic condition, only one side of the body is impaired. With diplegia, the lower limbs are more effected than the upper limbs; and with quadriplegia both arms and legs are equally

effected. The non-spastic section can be further sub-divided into ataxic, or loss of coordination, and dyskinetic, or impairment of involuntary movement. There are further divided classifications, but the scope of this research is to investigate the major classifications (Ken Stern, 1997).

The most universally accepted system, especially in research, is the "Gross Motor Function Classification System" or GMFCS. The motor functions are based on self-initiated, voluntary movements, generally referring to everyday movement such as sitting and walking. The classification system is divided into five distinct levels, with 1 being less impacted and 5 being most severe. The system is meant to represent the patients' abilities and limitations (including needing mobility devices). The general distinction between the levels is included below:

Level 1 patients can walk without limitations

Level 2 patients can walk, but with some limitations

Level 3 patients can walk with the assistance of a hand-held mobility device

Level 4 patients are mobile with the assistance of powered mobility device

Level 5 patients are mobile with external assistance in a manual wheelchair

The levels described are taken from the expanded and revised GMFCS review (R. Palisano et al., 2007 and 1997).

While the disorder originates from a neurological pathology, cerebral palsy symptoms are mainly muscular. Previous research in this lab and others have found evidence that the muscles themselves are being altered, in such ways as a decreased satellite cell population (Dayanidhi et al., 2015) and increase in sarcomere length – resulting in a change on the length-tension curve (Mathewson et al., 2014). In this study,

it is our hope that therapies focusing on treating clinical muscular fibrosis could also prove beneficial for patients with cerebral palsy and other muscular disorders.

Electron Microscopy

While collagen content itself has been studied numerous times in research, it is hard to capture visually. This is because light microscopy lacks the resolution necessary to visualize all aspects of collagen. Collagen fibers spans large distances, usually in terms of microns, but the finer details of the fibrils is in terms of nanometers. To get a good qualitative image of both of these resolutions, electron microscopy must be employed. Electron microscopy methods have been well established in biological tissues, particularly in skeletal muscle (Hall et al., 1946 and Huxley & Hanson, 1954). However, much of the work has been done on the interior structure of the contractile properties of muscle, and much less work has focused on the ECM, due to the restrictions mentioned above. Some electron microscopy techniques have been applied to ECM in previous work done by this lab, but the preparation methods proved harsh to the sample to the point of unquantifiable images. The typical scanning electron microscopy protocol cause an amount of shrinkage, meaning it was particularly difficulte to determine position and dimensions of the ECM. With the introduction of a newly developed three-dimensional imaging technique, we are now able to observe 3D ECM ultrastructure with *in vivo* morphology to allow for quantification of the collagen structure. This new technique, Serial Block Face Scanning Electron Microscopy (SBFSEM), combines finer resolution normally associated with TEM and the three-dimensional capacity of SEM (Denk & Horstmann, 2004). To our knowledge, this is the second application of SBFSEM on skeletal muscle ECM (Gillies et al., 2013) and the first application on human ECM.

II:

Materials and Methods

Mouse Perfusion Fixation

All work was approved according to UCSD IACUC policies prior to beginning. Mice were taken in conjunction with another graduate student's experiments in the lab (Chapman et al., 2014). Mice were desmin/nesprin1 double knockout mice, aged between 2 months and 8 months at time of perfusion. Typically two mice were perfused on the same day, according to the perfusion technique outlined in Deerinck et al., 2010, one wild-type (n=4) and one double knock-out mouse (n=7). All reagents were obtained from Electron Microscopy Sciences (Hartfield, PA). Mice were anesthetized with a 0.1ml/10g intraperitoneal injection of rodent cocktail (100 mg/kg ketamine, 10 mg/kg xylazine, and saline). Wild-type mice often needed twice as much of the anesthetic cocktail as the double knockout. When completely sedated, (tested with a toe and tail pinch), mice were perfused transcardially with mammalian Ringers solution and fixative containing: 2% formaldehyde (from paraformaldehyde), 2.5% glutaraldehyde, 0.2% dextrose, heparin (20 units/ml), 0.05% ruthenium red, and 0.2% tannic acid in 0.15M sodium cacodylate buffer containing 2mM calcium chloride, warmed to 37°C. The addition of the ruthenium red (Luft, 1971) and tannic acid enhance staining of the membrane and collagen fibrils for electron microscopy. Ruthenium red was added last to the mixture, and left to dissolve in 60°C for 5 minutes. Then the fixative was spun in an Eppendorf Centrifuge 5810R for 10 minutes at 25°C at 14,000 rpm. To ensure complete solubility, the fixative was then run through a vacuum filter. When the perfusion was complete, both soleus and tibialis anterior muscles were dissected out of either the left, right or both hind legs. Samples were incubated overnight in the same fixative at 4°C.

Biopsy Collection and Immersion Fixation

Before the use of human tissue, the perfusion fixation protocol was manipulated to allow for immersion fixation on mice. Fixative was prepared in the same fashion as the perfusion, with changes to the concentrations of formaldehyde and glutaraldehyde in combination. Mice were sacrificed via the cervical dislocation method, and then the soleus and TA were dissected out from both hind legs. The right hind leg (both muscles) was subjected to the perfusion fixative control 2% and 2.5% combination, while the left hind leg was subjected to the immersion experimental 4% and 1% combination (Wisse, 2010). In this sense, the mouse acted as its own control. After viewing Transmission Electron Microscopy (TEM) images, it was deemed that 4% formaldehyde and 1% glutaraldehyde were optimal concentrations for immersion fixation. Thus, almost all biopsy samples were immersed in this modified fixative mixture, unless adequate regent supplies were not available.

The biopsy study conformed to the ethical standards of the Institutional Review Board of the University of California, San Diego Human Research Protection Program. Biopsy CP samples were recruited from a patient with a developed contracture that required either hamstring lengthening surgery (n=2) or gastrocnemius-soleus lengthening (n=2). Control samples, defined as having no history of neurological disorders, were recruited from ACL reconstructive surgery with hamstring autograft (n=1) in partnership with Rady's Children's Hospital (IRB 111348 and 071702). All personal information obtained from consent forms of patients and parents was de-identified and associated with an identifier number. During surgery, samples were removed using an *in vivo* sarcomere length muscle clamp (Ward et al., 2009) and then stretched and pinned to 10-

15% greater than resting length before being left in ice cold fixative for 5 minutes (made fresh that day). After 5 minutes, the samples were cut into 1 mm^3 pieces using a sharpened razor blade. The sample was cut to increase the surface area and allow for further penetration of the fixative and heavy metal staining. At this point, the sample was transferred to fresh fixative and incubated for 2-4 hours at 4°C (including the ride back from the hospital) or overnight depending on the time of the surgery. An important note about CP and TD muscles are the patients' age; the average age was 9 years and 12 years respectively.

Biochemical Assays

For the purposes of this experiment, the collagen protein was detected and quantified through Western Blots and Enzyme Linked Immunosorbent Assays (ELISA). Frozen samples with known passive mechanical properties were taken from a previous study (Smith et al., 2011). To begin, samples were homogenized in a Caframo BDC2002 and added to lysis buffer. Total protein concentration was measured using a microBCA kit (Pierce, Rockford,IL). Then, samples were digested with pepsin for the Western Blots at various time frames of digestion, in order to find the optimal digestion time. Fifty micrograms of total protein were loaded on 7.5% SDS-PAGE. Proteins were separated at constant volts at 25 mAmps/gel. Gels were then transferred to a 0.45 μm nitrocellulose membrane at 97 mA. The membrane was then stained with Ponceau S staining solution to visualize transferred proteins. The membrane was blocked with 5% BSA in TBST (Tris buffered Saline pH 7.2) overnight at 4^0C. Blots were incubated with primary antibodies (Abcam Human type I and III collagen [1:5,000]) for 1 hour and then washed 3 times every 15 minutes with TBST, after which blots were incubated with horse-radish-

peroxidase (HRP) conjugated mouse secondary antibody (1:10,000) for 1 hour. The blots were washed every 15 minutes for 2 hrs. The membranes were then incubated in chemiluminescence (ECL) reagent for 7 minutes and imaged by X-ray as well as Imager (Bio-Rad).

Kits for ELISA were purchased from Chrondex for Type I, BlueGene for Type III, and Antibodies-Online for Type IV (Cat # ABIN1028401) and Type VI (Cat #AB1N509882). The general protocol provided by the kit was followed to quantify the concentration of each isoform. Each sample was tested in single count and compared to the serial standard concentrations given. Spectrophotometric measurements were taken with KC4 Data Analysis software. Total collagen concentration was measured via colorimetric hydroxyproline assay. Samples were hydrolyzed at high heat (110° C) in 6N HCl for 24 hours, after which samples were pipetted onto a well plate and added to Cholarmine T and p-diaminobenzaldehyde solution before incubation at 60° C for 1 hour. Plates were read at 550 nm in triplicate. Samples underwent analysis before and after digestion, as well as after the assay. Absorbances were used to calculate the mass of hydroxyproline in the sample, and thus determine the mass of collagen per mass of wet tissue. Calculations used a standard constant of 7.46, defined by the number of hydroxyproline residues in a molecule of collagen (Grant, 1964).

Electron Microscopy Staining and Preparation

It was our aim to employ a fairly new technique in three-dimensional reconstruction of muscle. Because collagen tendrils are known to be difficult to isolate, it requires high-resolution electron microscopy over millimeters to centimeters in length. This new technique made use of scanning-block face electron microscopy with

automated serial ultramicrotomy (Gillies et al., 2014). This allowed for continuous imaging over a large capacity of ECM.

After perfusion fixation or immersion fixation, tissues underwent post-staining with a modified osmium tetroxide protocol (West et al., 2010). Osmium (2%) was mixed with an additional ruthenium red (0.05%) supplement and potassium ferrocyanide (1.5%). Tissues were then washed in distilled water, incubated in 1% thiocarbohydrazide (TCH), and washed again before the 1% uranyl acetate incubation overnight. The next day, tissues were stained *en bloc* with lead aspartate and dehydrated in graded ethanol solutions. The final step involved embedding the tissues in Durcupan ACM resin (Sigma-Aldrich) and mounted on blocks or aluminum pins for thin sectioning (~70 nm) with a diamond knife. The processing procedure takes about a week to complete, from perfusion/immersion to embedding.

Samples were sectioned and trimmed using an ultramicrotome (Leica Ultracut UCT). Thin sections were viewed on a FEI Spirit TEM microscope under low magnification (2700-4400x) and analyzed with ImageJ. Samples that were deemed ready for 3View, based on the quality of the TEM images, were mounted on aluminum pins and trimmed to a 1 mm^3 rectangle with a glass knife, and coated with gold sputtering.

Fully processed specimens were loaded onto a Zeiss Sigma Scanning Electron Microscope (SEM) outfitted with the image-processing machine (Gatan 3View, Pleasanton, CA). The Digital Micrograph software (Gatan) controlled the diamond knife and specimen movement inside the Zeiss chamber to allow for specific section thickness and cutting speed (set to 0.5 mm/sec with oscillation). Images used a 3 kV accelerating electron high-tension voltage under variable pressure ranging between 19-30 Pa to offset

resin charging. The program then captures an image of each layer (70 nm thickness) at 2,400x magnification and raster size 10,000 x 10,000 with 1µs dwell time, and is able to stack them together. The stacks contain approximately 1,000-2,000 images, giving a total depth of 70-140 μm. Data acquisition for a single specimen took approximately 36 hours to run until completion, with the need for manual focus and stigmation adjustments occasionally. Pixel sizes required a separate imaging session with a calibration grid (Ted Pella Inc, Latex Calibration standard) and processed on ImageJ.

For analysis, images were stacked, aligned, and cross-correlated. Segmentation was performed manually with IMOD software (Kremer et al.,1995), and automatically with IMARIS. Objects are defined by stitching together similar contours on neighboring images, and then built up in voxel size and volume. Manual segmentation took approximately 40 hours for a complete reconstruction.

X-ray Microscopy

Data was collected on a Zeiss Versa 510 X-ray microscope, which operated at 80 kV and 7 W power for the purposes of this study. At least 30 minutes before imaging the microscope was allowed to stabilize with the source on. Imaging was performed using a 4X objective, and the sample was rotated 360° with 3200 tilt increments. Exposure time was 0.5 sec, with a total acquisition of 30 minutes. The resulting volume had 2.74 um isotropic voxel dimensions. Volume renderings were performed using Zeiss' XM3DViewer software and converted to a series of tiff images using Zeiss XMController software and ImageJ software. All X-ray microscopy was performed by Eric Bushong, all other microscopy was performed by myself.

III:

Results

All collagen isoforms are increased in cerebral palsy, but are unrelated to functional parameters

Samples for biochemical assays were frozen from the previous Smith 2011 study, and were chosen depending on tissue size. A summary of all the patients' and mice considerations can be found in Table 1 and Table 2 respectively. Only after all assays

Table 1: Patient Considerations. GMFCS is the system used to describe a child's self-initiated movement. GMFCS is not used to describe a patient who is typically developed (TD). The table is divided into two sections; the first section was samples used in biochemical assays, the second section was used in electron microscopy studies. Q = quadriplegic, D = diplegic, H = hemiplegic

Group	Surgery Type	Test Run	Avg Age	Avg GMFCS	Affliction	Male	Female	Total
Cerebral Palsy	Hamstring Lengthening	Biochemical	9.4	2.8	8 Q, 8 D, 1 H	10	7	17
Typically Developing	ACL reconstruction	Biochemical	15.8	N/A	N/A	8	10	18
Cerebral Palsy	Hamstring Lengthening	Microscopy	7.5	3.25	2 D, 2 Q	1	3	4
Typically Developing	ACL reconstruction	Microscopy	16.0	N/A	N/A	0	1	1

Table 2: Murine Considerations. The table above lists the condition, age and test run on each mouse group, specifically denoting which muscles were tested. WT = wild type, DKO = nesprin/desmin double knockout, TA = tibialis anterior

Group	Affliction	Muscle	Avg Age	Test Run
Group 2	WT and DKO	Soleus	6.5 mo	Perfusion/Dissection practice
Group 3	WT and DKO	Soleus and TA	8.5 mo	Microscopy
Group 5	Desmin KO	Soleus and TA	12 mo	Immersion practice
Group 6	DKO	Soleus and TA	2 mo	Microscopy
Group 7	WT and DKO	Soleus and TA	4.25 mo	Microscopy
Group 8	DKO	TA	6 mo	Microscopy

were performed, were the tissue samples related to the associated passive mechanics values of the previous study, so as not to bias the results. In Table 1, of particular interest are the categories for age and GMFCS (Gross Motor Function Classification System). It was difficult to relate muscle morphology of typically developing and cerebral palsy patients, as the difference in ages was quite pronounced. This difference is especially important when considering these two age groups are still largely in muscular development stages, and these stages largely depend on muscular use. This age difference was taken into account during all group comparisons.

Collagen concentrations, measured both by hydroxyproline and ELISA assays, for all isoforms are shown in Figure 2. The hydroxyproline assay revealed a significant increase in total collagen content in the CP samples, as was to be expected based on previous data (Figure 2A). Type I comprised most of the total collagen and seemed to show a marked increased in CP as compared to TD. However, when the results were fit to an ANOVA model between collagen content and stiffness, there was no statistical significance and a low confidence level (Figure 2C). Stiffness was taken from a passive mechanical test performed previously by Smith (2011). Type III, IV, and Type VI seemed to show a noticeable, albeit smaller, increase between the two patient groups. Data is presented with standard error (SEM) bars unless otherwise noted. It should be mentioned that ELISA measures only soluble collagen, whereas hydroxyproline measures all collagen; thus the concentrations values between the two assays (in Figure 2A) should not be compared. From the hydroxyproline and ELISA data, the estimated percentage of each isoform in the whole sample was calculated by taking the concentration of one isoform and dividing by the total concentration of collagen tested (ug/mg tissue).

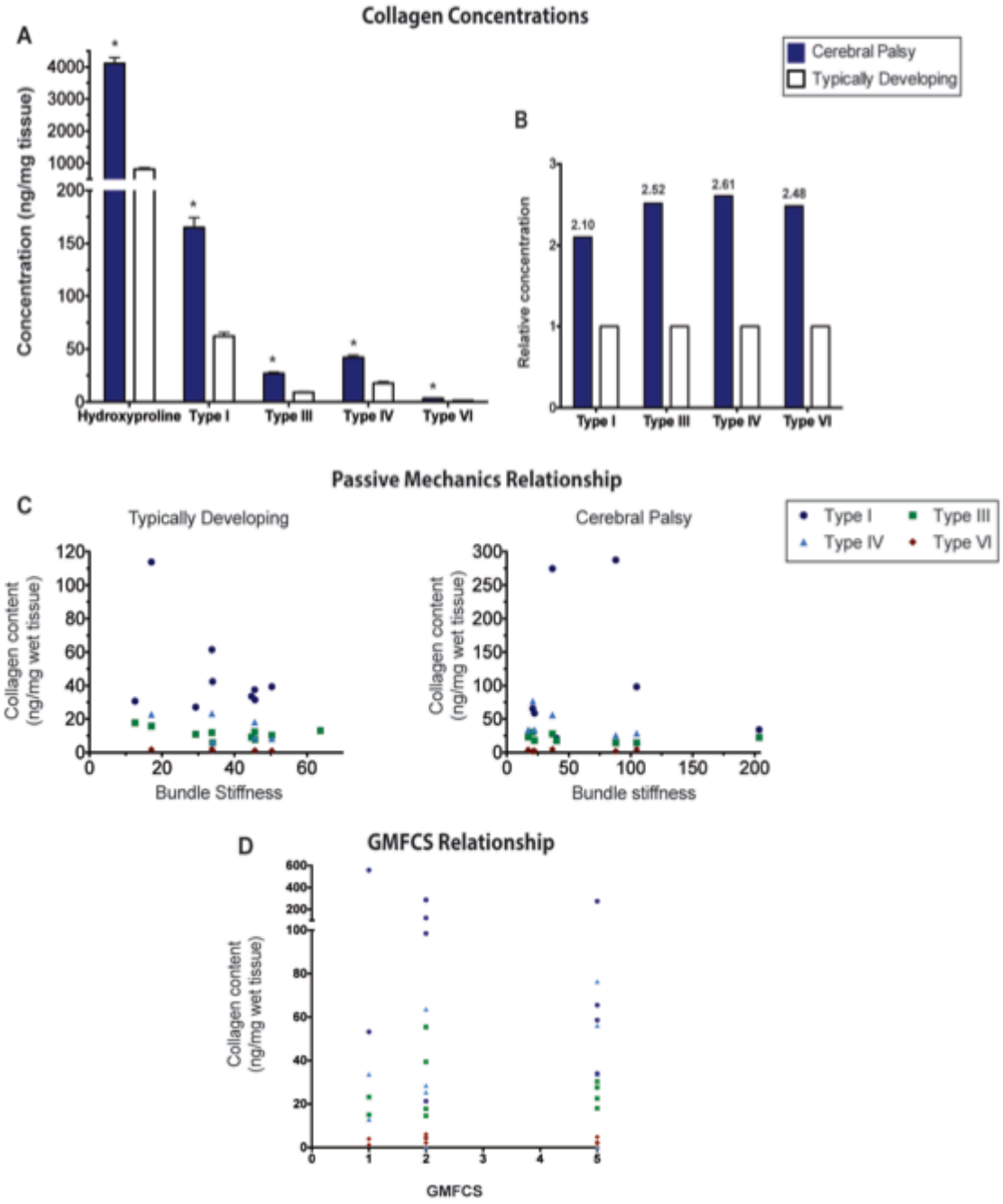

Figure 2: Collagen isoform concentrations are increased proportionally in CP. A shows the measurements of the hydroxyproline concentration (in ng per mg of wet tissue) and ELISA results of all isoforms. Type I, Type III, Type IV and Type VI were all statistically significant ($p < 0.05$, $p < 0.005$, $p < 0.05$, $p < 0.005$ respectively). B shows the relative increase of all collagen isoforms; values were normalized to the TD values. C correlates the collagen concentrations (for each individual isoform) to the passive mechanical properties of the muscle (NS). D corresponds collagen concentrations of each isoform to GMFCS (NS).

We noticed that there was a much higher concentration of Type I, so an isoform ratio comparison between the patient groups was plotted. In this comparison, we found that all four isoforms have approximately a 2.46 ± 0.19 fold increase in muscles with cerebral palsy (Figure 2B). Another comparison shows that while all isoforms are increased, they are only increased in relative proportions to concentrations found in typically developed patients (data not shown). To be clear, these isoforms are not found in equivalent concentration values; Type I is in hundreds on nanograms while Type VI is found in only ones of nanograms. But the ratio of Type I to Type VI is virtually equivalent no matter the condition of the muscle.

Lastly, we attempted to find a predictable correlation between collagen concentration and severity of the condition (using the GMFCS as a proxy of severity). Unfortunately, we could not find any correlation between the two (Figure 2D). It would appear that collagen concentration is a not a good indicator of severity of cerebral palsy, likely because there are other biochemical and physiological elements at play. Additionally, collagen isoforms appear insignificant in predicting an increase in stiffness. After this result, we re-focused our hypothesis concerning the basis of stiffness in CP from collagen isoforms to collagen structure. Our adjusted hypothesis lies with the idea that perhaps total collagen content does not tell the whole story, but rather how the collagen is orientated on the muscle that correlates with muscle dysfunction.

Introduction of New Protocol for Immersion Fixation of Human Samples

Before this particular project started, a murine protocol for electron microscopy had already been established and was under review for publication. The perfusion protocol needed to be adapted slightly for the purposes of this project, specifically in the

addition of ruthenium red to aid in the staining of collagen and basal lamina. Preliminary attempts on the adapted protocol revealed the need to adjust the manner in which the ruthenium red was added to the fixative. Before the adjustments the ruthenium red, added last to the fixative, would not dissolve in the solution. This meant that large amounts of ruthenium crystals were clogging the fixation lines and mouse vasculature. To overcome this obstacle, the protocol was reverted back to more resemble the original Luft protocol. The fixative was prepared, with ruthenium red added last, and the solution temperature was brought up to 60°C. It should be noted that the crystals were more readily dissolved while the solution was kept hot; but when the crystals would came out of the solution when cooled down. For the mouse perfusions it was possible to keep the solution warmed right up until the time of perfusion permitting us to use a solution that was mostly dissolved. Yet, this temporary solution consistency created an unsolvable problem for the immersion fixation protocol described next.

The immersion fixation protocol was first performed on murine samples, before testing on human patient samples. As aforementioned, the only major changes from the perfusion fixation protocol were in the concentrations of formaldehyde and glutaraldehyde. Because the concentration of formaldehyde was increased, there needed to be a decrease in glutaraldehyde. Fixed samples were checked through TEM images for completion of fixation (Figure 3A-B). All other aspects of the fixation process were kept constant to minimize side effects of other variables. While both concentrations gave fairly sustainable results, the samples that underwent the experimental condition had better results over more of the sections imaged. A larger percentage of myofibers in the experimental condition had clear membrane and collagen staining, with better aligned

sarcomeres. The sarcomeres and structures had cleaner outlines and more defined structures, and from these imaged it was deemed that the experimental condition would be tested on the first human sample.

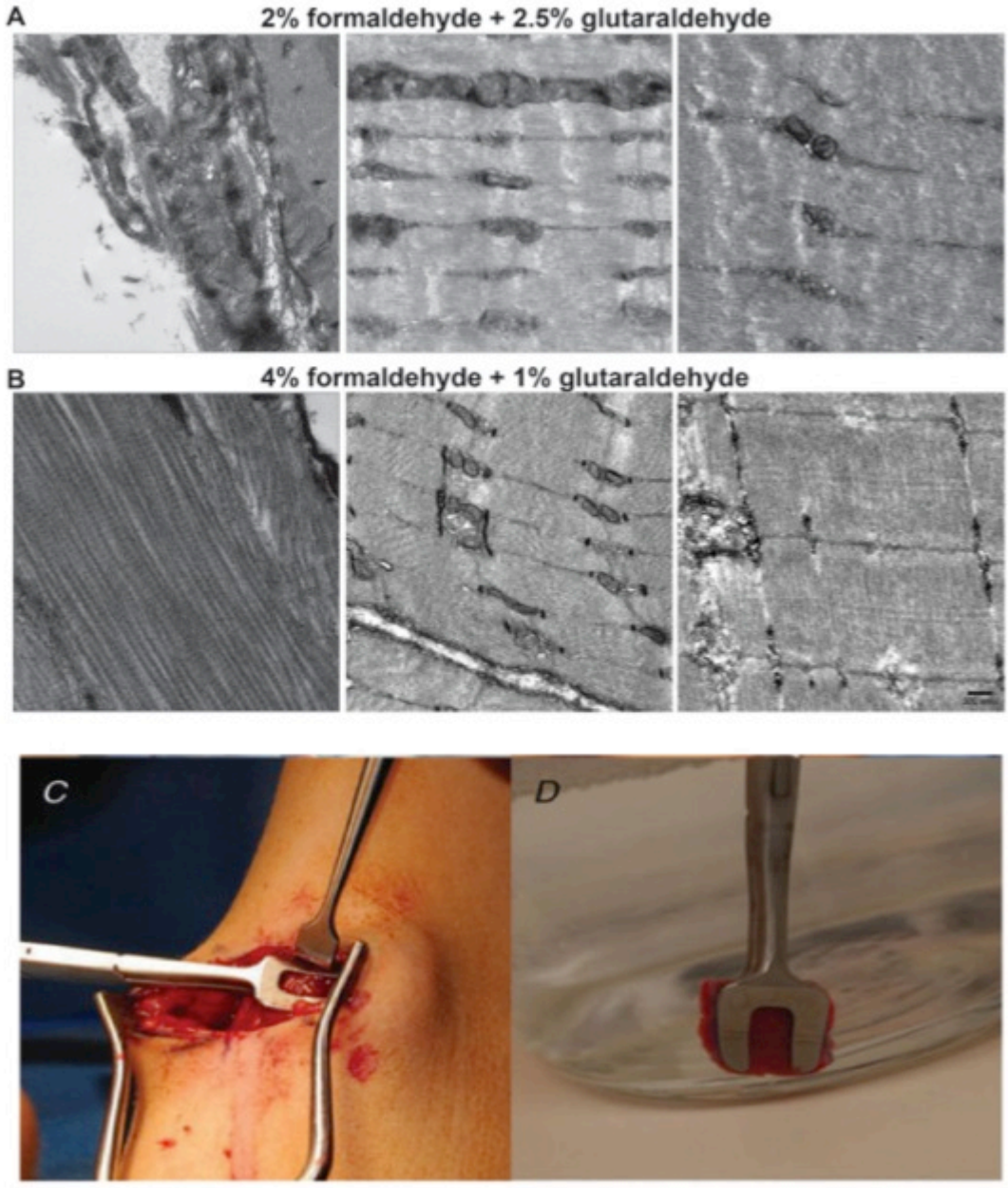

Figure 3: Developing a new immersion fixation protocol. A is TEM images of mice with the 2% formaldehyde and 2.5% glutaraldehyde fixation. B is TEM images of mice with the 4% formaldehyde and 1% glutaraldehyde fixation. Scale bars are shown on the right image in B. C-D show the biopsy clamp with muscle taken from a surgery. Image taken from Smith et al., 2011, fig 1.

Next, the new protocol was tried on a typically developing sample. The use of a validated biopsy clamp (Figure 3C-D) allowed for the muscle to be removed at *in vivo* lengths (Ward et al., 2009). But to better appreciate the structures and ultrastructures we were interested in, we stretched the muscle to 10-15% past the *in vivo* length. The sample was pre-fixed at this length for 5 minutes in ice-cold fixative. Because the fixative was kept at a colder temperature (necessary for the fixation process), it was not clear how much ruthenium red was in solution and how much was out of solution. However, looking at TEM images of the typically developing sample (Figure 5), the basal lamina and collagen were both heavily stained, indicating that the ruthenium red was indeed present. After the first human sample was deemed fit for SEM, the immersion fixation protocol was characterized as complete and ready for cerebral palsy samples.

Serial Block Face Scanning Electron Microscopy and Transmission Electron Microscopy were used to characterize ultrastructural differences between Wild-Type and Double Knockout (DKO)

A comparison of both mice used, wild-type and double knockout, are shown on TEM in Figure 4A. At first look of these images, it was noted that the amount of collagen was in fact increased in the double knockout mice, as expected. However, the major difference in collagen wasn't the amount but the network. In wild-type, the perimysium collagen was fibrillar and disperse. There were patches of fibrillar clustering, but each fibril was still clearly outlined as a separate entity. On the other hand, in double knockout the collagen was packed so densely that it became impossible to distinguish the fibrils of collagen. In some cases, the micrographs showed a dark outline of the collagen, indicating layers of dense packing. It was not clear from these micrographs whether the

increased packing of collagen was due to cross-linking changes or extracellular proteins changing. The graduate student these mice belonged to performed the experiments looking into these questions. It was found that collagen cross-links were not significantly changed in double knockout mice. But looking into the array of cells that can produce collagen, a variety of cells were increased. The cells were divided into three main groups, fibro-adipogenic progenitor cells (FAPs), skeletal muscle progenitor cells (SMPs), and miscellaneous cells (were not clearly identified with the labeling used). It appears that FAPs and miscellaneous (including fibroblasts) were increased in expression, rather than collagen expression increasing from the same number of cells. This leads into more work on growth signals likely contributing to this increase in expression. A depiction of each individual animal can be found in the supplemental figures (S1-S2).

In some areas spotted, the increased collagen created a small disruption in the muscle fiber orientation. These disruptions were more easily spotted on the SEM images (Figure 4B). It appeared that the collagen assembly was either pushing the fibers out of the way or encasing the fibers, and thus disrupting the network of muscle fibers. To have this kind of restriction on the muscle fiber, functional efficiency of the sliding contraction myofibrils is certainly decreased. Collagen was also found in high amounts surrounding the neuromuscular spindle, possibly creating a situation in which the electrical signal is being dimmed. More work would have to be done on this idea.

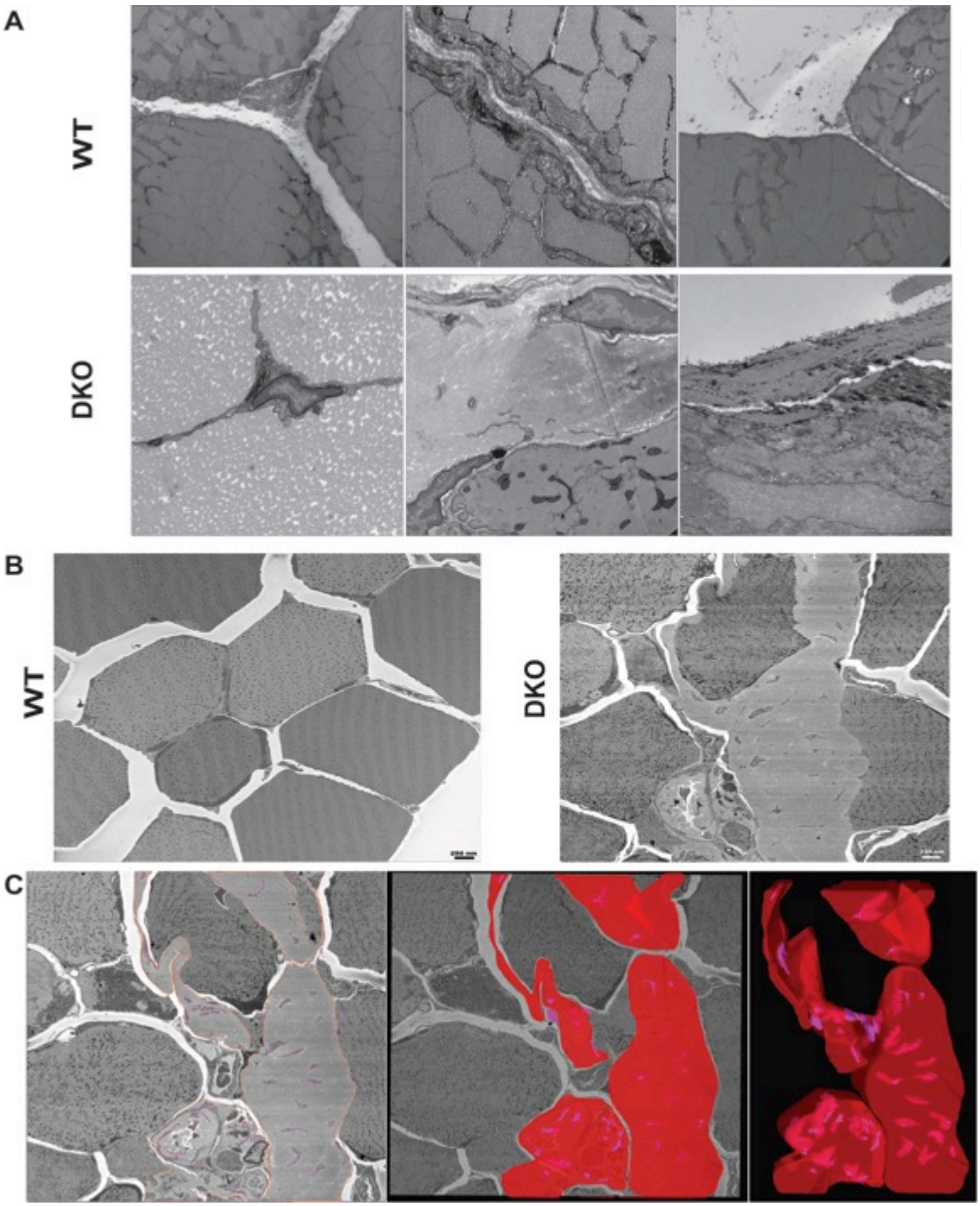

Figure 4: Comparisons of wild-type and double knockout mice. A shows TEM images of WT and DKO, highlighting perimysium collagen packing differences especially around the basal lamina. B shows SEM images used in 3View reconstructions. Scale bars on B represent 250 nm. C illustrates how IMOD uses stacks of SEM images to manually segment structures, giving the overall reconstruction in the last panel. Red = collagen, Pink = fibroblast

Reconstructions show the increase in fibroblast number and collagen packing (Figure 4C). The image on the left shows the SEM micrographs used in manual segmentation with the IMOD software. Structures ("Objects") were traced every few slices ("contours"), depending on what was being traced. Myofibers, which changed fairly modestly throughout the stack, only required tracing every 100 slices and were merged together in the reconstruction. Vasculature had some more moderate changes with possible branching, and so were traced a little more regularly, approximately every 50 slices or so before being merged together. Collagen and fibroblasts were highly branched and would often stop and start abruptly, and thus were traced every 10-25 slices. If it was particularly difficult to merge, as the fibroblast projections ("processes") were long and thin, then the traces were interpolated before merging. Interpolated traces were carefully inspected on every slice, as the program would often misinterpret the trace and would have to be corrected manually and re-interpolated.

Serial Block Face Scanning Electron Microscopy and Transmission Electron Microscopy Were Used to Characterize Differences Between Typically Developing and Cerebral Palsy Patients

First, a typically developing sample underwent the initial immersion fixation protocol. Before a cerebral palsy sample underwent the same protocol, the typically developing sample was inspected by TEM (Figure 5A). It is rare to find typically developing human electron micrographs, as most experiments do not get permission for such things. As such, there was a low amount of research to compare these micrographs to. However, with the expertise of the Ellisman lab, it became evident that these micrographs were in reasonable condition and fixed as best as possible for these

purposes. Multiple organelles and structures could be clearly denoted in the images, as labeled in Figure 5 and Supplemental Figure 3 (S3).

Four separate cerebral palsy biopsies, consisting of four muscle types, were collected in the time frame of this study. However, due to time constraints, only three of the biopsies will be presented in this thesis. Due to patient confidentiality, the samples will henceforth be known as CP patient 1, CP patient 2 and CP patient 3. As with any disorder, and as noted in the introduction, each patient is unique in their symptoms. Thus it is difficult to proclaim one sweeping statement about cerebral palsy simply by looking at these three samples. But they are the first of their kind and still do provide some insight into a world researchers know little about.

Both SEM and TEM micrographs comparing typically developing and cerebral palsy patients can be found in Figure 5 and Supplemental figures 3-6 (S3-6). While the typically developing images are meant to showcase all aspects of muscles, the cerebral palsy images are explicitly focused on fibroblast projections and collagen packing. When using the transmission electron microscope, it was generally easy to find areas of excessive collagen packing in cerebral palsy samples (Figure 5A). Most often, these areas of collagen were encapsulated by fibroblasts (or similar, but unidentified cells) with extremely long projections. As can be seen in most of the images portraying collagen, while the myofiber is cross-sectional, the collagen fibrils can be found as cross-sectional or longitudinal. This is because the fibrils are not restricted to one plane, but extend in all directions and in all orientations. This is not uncommon and not an abnormality associated with cerebral palsy.

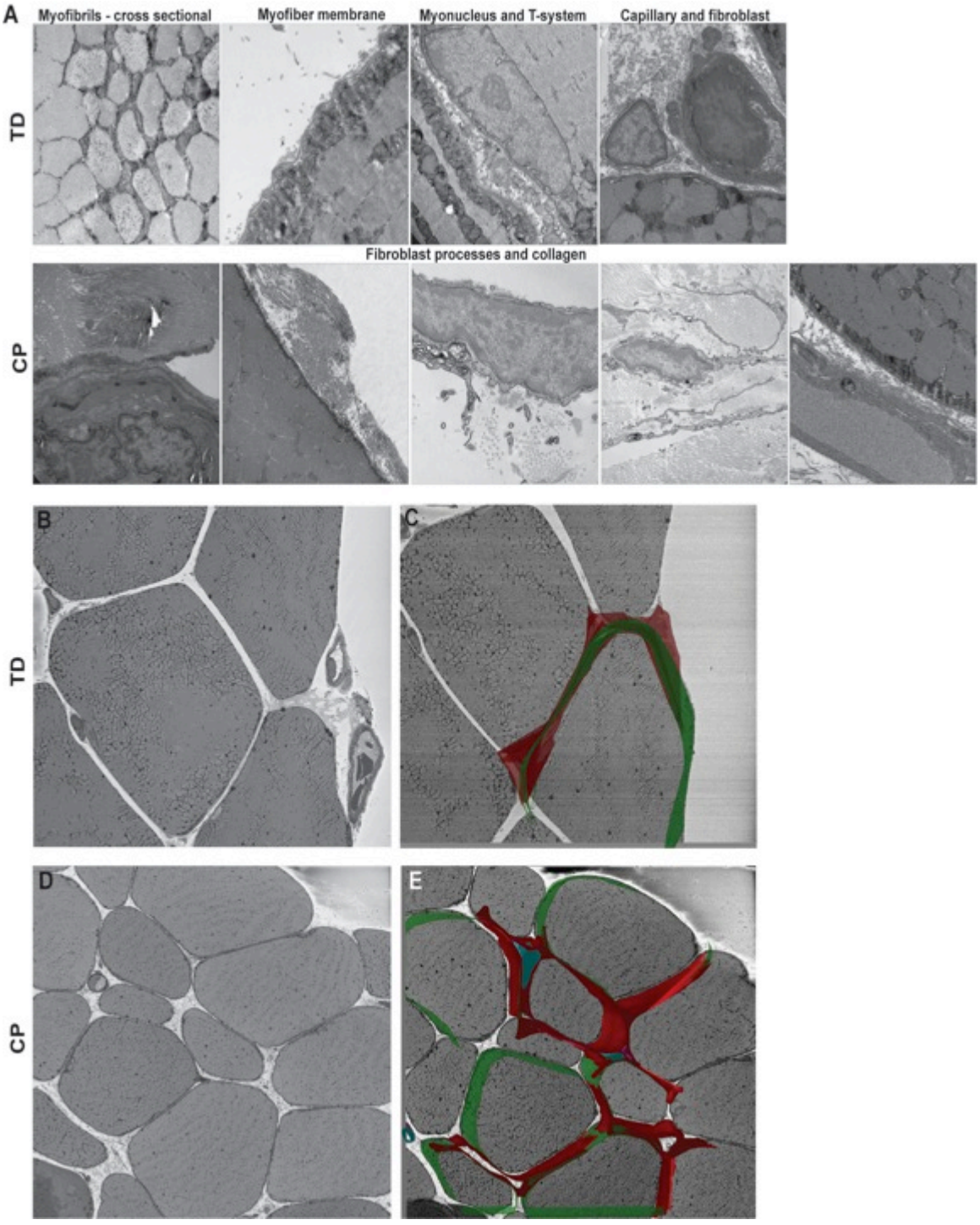

Figure 5: Comparisons of typically developing and cerebral palsy patients. A shows TEM images, with headers explaining the structures. B-C shows SEM of TD and the reconstruction of perimysium collagen around a myofiber. D-E shows SEM of CP and the perimysium collagen around multiple myofibers. B-E magnification = 2400x. Red = collagen, Green = myofiber, Blue = capillary

One key difference between typically developing and cerebral palsy is how the fibrils appeared on CP images. The fibrils visually appeared to have a slightly thicker diameter (not quantified) and more often found in larger, concentrated bundles. However, this trend was not as easily seen in the SEM images. It could be a sampling problem and would be more obvious with more areas of interest in the 3 samples tested, or simply more samples need to be tested.

During our study, there was an abnormality that we were not expecting to find, but continued to show up in every CP sample we imaged. We are still unsure of what to make of the abnormality, but it appears to be worthwhile to look into. It first appeared in the SEM video of CP patient 1. It looked like the myofibrils in multiple myofibers were switching between cross-sectional and longitudinal (Figure 6). While this is normal for collagen (as explained above), this is unheard of for myofibrils. The muscle itself is set up very explicitly to produce force through one specific pathway. With this orientation we witnessed, the question arose of how a muscle such as this would be able to contract. Figure 5A attempts to answer this question. After seeing this myofibril abnormality, we investigated further by looking at higher magnification with TEM. Not only did we find both longitudinal and cross-sectional myofibrils in the same myofiber in this patient, we found a distinct “transition zone” between the two myofibril orientations in CP patient 1 and CP patient 2 (Figure 6B). CP patient 3 has not been evaluated yet on TEM to find a “transition zone”, however the abnormality was present in one of the myofibers on SEM.

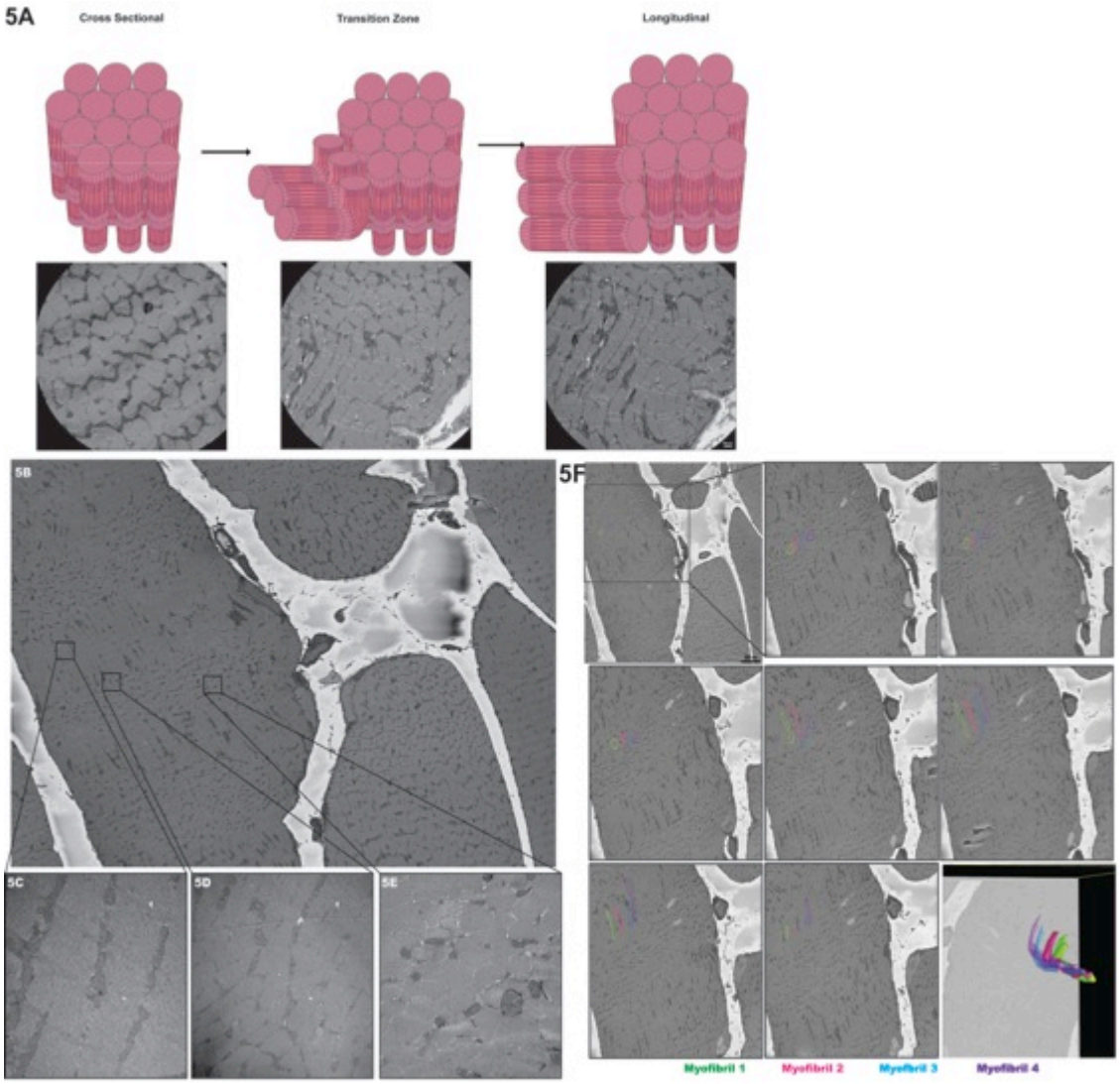

Figure 6: Changing myofibril orientation within myofibers. A shows our depictions of what might be happening on the myofibril level coupled with TEM images of what we actually observed (which helped in creating our depictions). B-E shows more TEM images that are higher magnification of SEM images in which were first observed this abnormality. F panels our numerous tracings and eventual reconstruction of the myofibrils. Video can be found in the supplementary files.

Reconstructions were helpful in visualizing how the myofibril orientation might look in the whole myofiber. We originally had two theories for how the orientation might stretch along the whole myofiber. But the reconstructions seem to point to our second theory, in which the myofibrils start out as one orientation, and then bend into another

orientation (Figure 6C). It is unclear whether the myofibrils ever curve back into their original orientation or remain bent. More reconstructions should help with this question. We are also uncertain as to why this happens, but these images likely won't give a satisfactory answer. Rather, we will need more experiments and imaging to get a sense of what or why this happens.

Correlating TEM with X-ray Microscopy with SEM data

To better correlate an area of interest found through TEM into our SEM 3View videos, a fairly new X-ray microscopy technique was utilized. The first visualization tool used on any sample was TEM (Figure 7A), to get a sense of the staining and fixation. During these checks, we also searched around for areas of interest for the SEM 3View videos. However, it was difficult to relate an area of the block face found on TEM to what we saw on the SEM images, especially since the block had to be trimmed down to 1 mm^3 between the two microscopes. With the images taken from X-ray, we were able to visualize the entire sample block to manually locate good areas of heavy metal staining or areas of interest in terms of ECM. From here, we could tailor-trim the block to focus in on the area of interest. As long as the block face itself was not trimmed too much between the X-ray microscope and SEM, we were able to use the X-ray videos to find the area in our SEM images (Figure 7B-C). Before the introduction of this technique, trimming the block and imaging with SEM could be a shot in the dark in terms of finding a well-stained, interesting area. It was hard to know if the SEM image would continue to cover the area of interest, or if the area would move. The advent of this technology gives a greater scope of the whole block before fitting it to the microtome on the SEM.

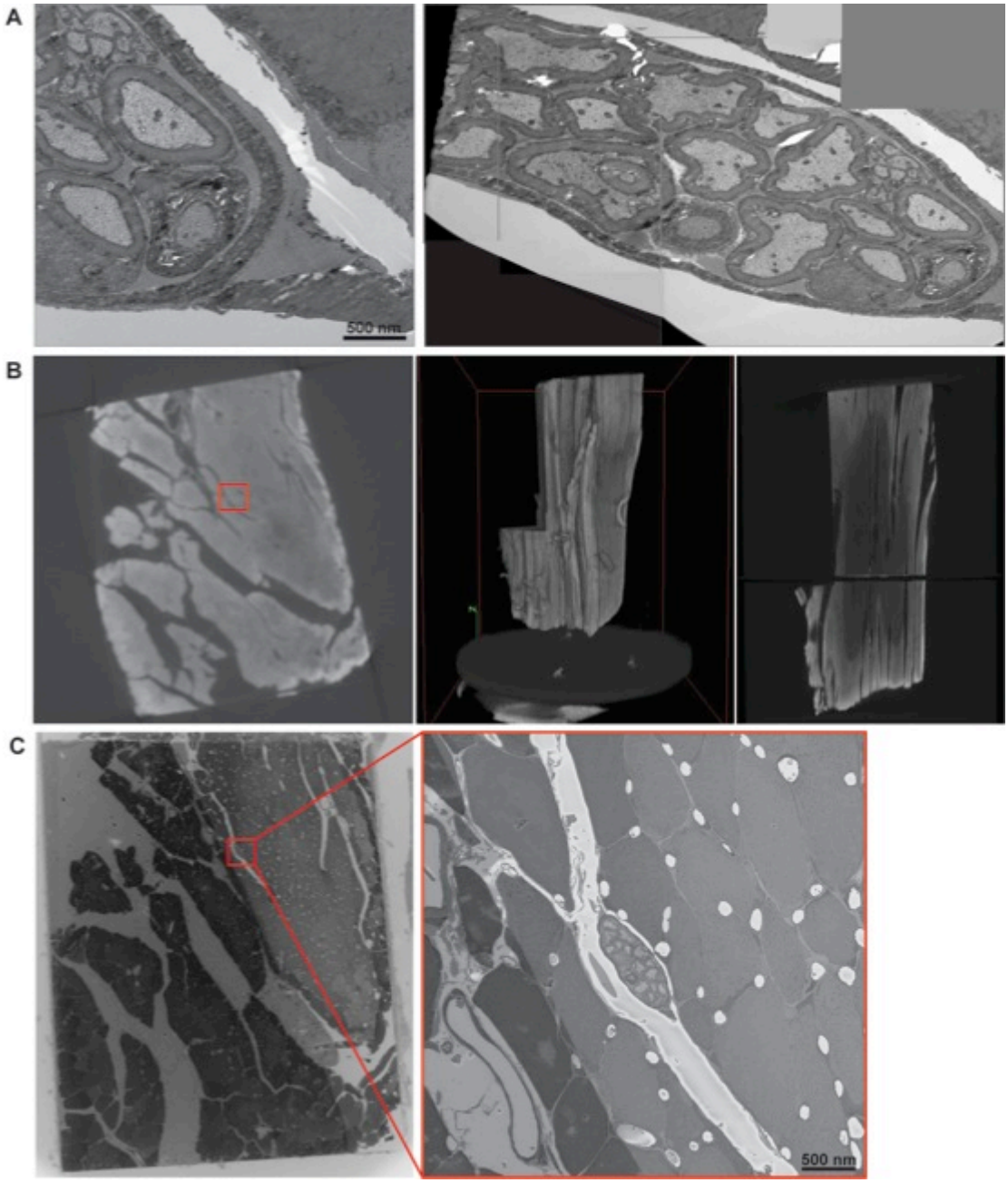

Figure 7: **Correlation of area of interest found in TEM to X-ray to SEM.** A shows an area of interest found in TEM, a myelinated nerve surrounded by collagen. B shows the X-ray micrograph of the block face, with the nerve boxed in red, and two 3D renditions of the block. The middle micrograph shows a volume rendition and the right micrograph shows an orthoslice rendition, in which the lighter areas show good heavy metal staining. C shows the SEM image of the block face, with the nerve outline. The inlet shows a zoom in of the nerve and the image used for SEM 3View.

IV:

Discussion

This project focused on understanding the extracellular matrix of two separate fibrotic conditions in two separate species. The reason for studying the extracellular matrix of cerebral palsy came first with the idea to explore the molecular basis for muscular stiffness found in the majority of patients. Data looking solely at the muscular alterations could not fully explain the increase in stiffness. Because muscle has a complex structure-function relationship, all aspects of muscle structure should be analyzed in regards to diseased states. While the extracellular matrix often goes unnoticed in these studies, we decided to focus mainly on the change in concentrations and network organization of extracellular components, specifically collagen. With insights gained from these experiments, we would be able to expand our knowledge to possible treatments or therapies for future research.

However, it is difficult to directly ask the question behind possible fibrosis in a diseased state, particularly when the samples used are human and subject to wide variability. Therefore, we used other accessible model systems to our advantage. A fellow graduate student was kind enough to allow us to take his fibrotic mice for our EM protocols. With a new model system in our hands, we were able to expand our viewpoint outwards and examine all aspects of skeletal muscle fibrosis in order to answer our questions. What was found in our animal models cannot be directly applied to the cerebral palsy conditions, but is used instead as a stepping stool in our understanding of this vastly heterogeneous condition.

Skeletal muscle fibrosis has already been defined in previous literature, but pathways involved are still not completely understood. There were two possible pathways for increase in collagen, either the same number of cells received signals to synthesize

more collagen or there were signals to produce more cells, each synthesizing the usual amount of collagen. What we found in our model, though certainly not a universal fibrosis model, was an increase in fibro-adipogenic cells and fibroblasts (found through FACS by the graduate student). It appears to be that these collagen-making cells are actually increased in numbers. It is not clear from the scope of this project where these signals are coming from but qualitatively the micrographs show an increase in fibroblast numbers. As of now we can't compare this trend to cerebral palsy, but future research will work to test this hypothesis.

In this work, we have created the first-ever immersion fixation protocol for human skeletal muscles used in electron microscopy. Not only was the fixation process successful, but also the staining for electron microscopy additionally proved successful, as depicted in both TEM and SEM micrographs. With this protocol, we can now compare a typically developing individual (images of which are rare to find in the electron microscopy world) to any other individual with a certain disorder, in order to evaluate differences between healthy and diseased tissues. This work paves the way for a multitude of new EM studies with human skeletal muscles.

The idea for this project would not have been possible without previous work (Gillies et al., 2013) examining skeletal muscle and ECM. With the knowledge of SBFSEM successes, we aimed to increase the range of tissues to use with SBFSEM. First, the question became how to best visualize ECM, which required a more delicate fixing and staining process to retain *in vivo* structures. Ruthenium Red, in addition to the already established tannic acid, seemed to be the best candidate for the case. A little tweaking was needed before ruthenium red could be used consistently in perfusion and

immersion. Next, the project focused on fixing human tissue for electron microscopy. However, the previous perfusion fixation method would no longer be viable in this condition. Thus, the perfusion protocol had to be adapted slightly before it could be possible to use for human tissue. After literature research and advice from experienced individuals in the microscopy field, the protocol was ready for testing on human tissue. The first sample tried, a typically developing patient, showed almost perfect fixation and staining; the best possible fixation without perfusion. It was now possible to compare side-by-side images of animal (mouse models) and human tissues.

The resolution used in SBFSEM spanned hundred of microns and was able to showcase perimysium collagen cables in reference to known structures such as capillaries and myofibers. In particular, it was possible to observe the relationship between collagen cables and fibroblasts. These images come in handy when discussing fibrosis and fibroblast regulation. It was now possible to qualify fibroblast concentrations in comparison to collagen concentrations. Whereas the question used to be if fibroblasts were increased in concentration, or if they simply received a signal to increase collagen production; we are now able to determine the likely possibility of the former option. If this were to be the case in every fibrosis condition, it would mean a breakthrough in targeting therapies.

When looking at the muscle structure itself, there have also been some insights not previously described. First, simply looking at the shape of the myofibers. Qualitatively, from the small sample size provided, it seems that the typically developing myofibers are larger with more of a rhomboid shape. However, the cerebral palsy myofibers have a trend towards a small size, with a more circular shape. This will be

looked into more with further investigations. Additionally, the myofibrils proved to have an unexpected orientation in some of the cerebral palsy muscles we sampled. This phenomenon was best appreciated in the 3View videos, where it was possible to watch myofibrils start out in the cross-sectional orientation, and then switch into the longitudinal orientation. Reconstructions allowed us to visualize how this might be occurring in the myofiber, and give us a diagram depiction (Figure 6). It is as of yet unclear whether this switch in orientation is indeed an abnormality found only in cerebral palsy, and what might be causing it. If in fact it is the disorder causing the orientation switch, it would require a loss of skeletal muscle structural proteins, such as desmin. However, data on cerebral palsy does not seem to indicate that desmin is nonfunctional in these patients, and so there may be another player to look into.

All of these data together are not strong to proclaim one general conclusion on muscle stiffness, but each data set points to a new direction to head for future experiments. First, we exhibit that collagen isoform concentrations are not the problem in the fibrotic-like situation found in cerebral palsy. Increases in collagen do seem to be a symptom of stiffness, but it is still unclear as to the functional implications of the increase. However, the answer may lie in the structure, as the collagen packing appears to be more pronounced in fibrosis models of both species. If the cause of this packing density in cerebral palsy is similar to the change found in fibrotic mice (fibrosis initiated by desmin/nesprin knockout), then we should be looking further into fibroblasts and other collagen-synthesizing proteins in the extracellular matrix as our answer for the collagen increase in cerebral palsy. If this turns out to be the functional difference between the

typically developing muscles and their stiffer counterparts found in cerebral palsy, we have a new aim for future treatments.

REFERENCES

Chapman, M. a, Zhang, J., Banerjee, I., Guo, L. T., Zhang, Z., Shelton, G. D., … Chen, J. (2014). Disruption of both nesprin 1 and desmin results in nuclear anchorage defects and fibrosis in skeletal muscle. *Human Molecular Genetics*, 1–14. doi:10.1093/hmg/ddu310

Crenna, P. (1998). Spasticity and " Spastic " Gait in Children with Cerebral Palsy. *Neuroscience and Biobehavioral Reviews*, *22*(4), 571–578.

Dayanidhi, S., Dykstra, P. B., Lyubasyuk, V., McKay, B. R., Chambers, H. G., & Lieber, R. L. (2015). Reduced satellite cell number in situ in muscular contractures from children with cerebral palsy. *Journal of Orthopaedic Research : Official Publication of the Orthopaedic Research Society*, (July), 1039–1045. doi:10.1002/jor.22860

Deerinck, T. J., Bushong, E. A., Thor, A., & Ellisman, M. H. (2010). Ncmir methods for 3d em : a new protocol for preparation of biological specimens for serial block face scanning electron microscopy, 6–8.

Denk, W., & Horstmann, H. (2004). Serial block-face scanning electron microscopy to reconstruct three-dimensional tissue nanostructure. *PLoS Biology*, *2*(11), e329. doi:10.1371/journal.pbio.0020329

Gelse, K. (2003). Collagens—structure, function, and biosynthesis. *Advanced Drug Delivery Reviews*, *55*(12), 1531–1546. doi:10.1016/j.addr.2003.08.002

Gillies, A., Bushong, E., Deernick, T., Ellisman, M. H., & Lieber. (2014). Three-dimensional reconstruction of skeletal muscle extracellular matrix ultrastructure. *Microscopy and …*, *20*(6), 1835–1840. doi:10.1017/S1431927614013300.Three-dimensional

Grant, R. (1964). Technical methods Estimation of hydroxyproline by the AutoAnalyser. *Journal of Clinical Pathology*, *17*(6), 685–686.

Kremer, J. R., Mastronarde, D. N., & McIntosh, J. R. (1995). Computer visualization of three-dimensional image data using IMOD. *Journal of Structural Biology*. doi:10.1006/jsbi.1996.0013

Lieber, R., Runesson, E., Einarsson, F., & Friden, J. (2003). Inferior mechanical properties of spastic muscle bundles due to hypertrophic but compromised extracellular matrix material. *Muscle & Nerve*, *28*(October), 464–471.

Luft, J. H. (1971). Hemistry8 purification8 methods of use for electron microscopy and mechanism of action. *Anatomical Record*, *171*, 347–368.

Mann, C. J., Perdiguero, E., Kharraz, Y., Aguilar, S., Pessina, P., Serrano, A. L., & Muñoz-Cánoves, P. (2011). Aberrant repair and fibrosis development in skeletal muscle. *Skeletal Muscle*, *1*(1), 21. doi:10.1186/2044-5040-1-21

Meyer, G. a, & Lieber, R. L. (2011). Elucidation of extracellular matrix mechanics from muscle fibers and fiber bundles. *Journal of Biomechanics*, *44*(4), 771–3. doi:10.1016/j.jbiomech.2010.10.044

Palisano, R. R., Rosenbaum, P., Bartlett, D., & Livingston, M. (2007). GMFCS – Gross Motor Function Classification System Expanded and Revised, 1–4.

Palisano, R., Rosenbaum, P., Walter, S., Russel, D., Wood, E., & Galappi, B. (1997). Development and reliability of a system to classifcy gross motor function in children with cerebral palsy. *Developmental Medicine and Child Neurology*, *39*(2), 214–223.

Prado, L. G., Makarenko, I., Andresen, C., Krüger, M., Opitz, C. a, & Linke, W. a. (2005). Isoform diversity of giant proteins in relation to passive and active contractile properties of rabbit skeletal muscles. *The Journal of General Physiology*, *126*(5), 461–80. doi:10.1085/jgp.200509364

Smith, L. R., Chambers, H. G., Subramaniam, S., & Lieber, R. L. (2012). Transcriptional abnormalities of hamstring muscle contractures in children with cerebral palsy. *PloS One*, *7*(8), e40686. doi:10.1371/journal.pone.0040686

Smith, L. R., Lee, K. S., Ward, S. R., Chambers, H. G., & Lieber, R. L. (2011). Hamstring contractures in children with spastic cerebral palsy result from a stiffer extracellular matrix and increased in vivo sarcomere length. *The Journal of Physiology*, *589*(Pt 10), 2625–39. doi:10.1113/jphysiol.2010.203364

Urciuolo, A., Quarta, M., Morbidoni, V., Gattazzo, F., Molon, S., Grumati, P., … Bonaldo, P. (2013). Collagen VI regulates satellite cell self-renewal and muscle regeneration. *Nature Communications*, *4*(May), 1964. doi:10.1038/ncomms2964

Ward, S. R., Takahashi, M., Winters, T. M., Kwan, A., & Lieber, R. L. (2009). A novel muscle biopsy clamp yields accurate in vivo sarcomere length values. *Journal of Biomechanics*, *42*(2), 193–6. doi:10.1016/j.jbiomech.2008.10.004

West, J. B., Fu, Z., Deerinck, T. J., Mackey, M. R., Obayashi, J. T., & Ellisman, M. H. (2010). Structure-function studies of blood and air capillaries in chicken lung using 3D electron microscopy. *Respiratory Physiology & Neurobiology*, *170*(2), 202–9. doi:10.1016/j.resp.2009.12.010

Wisse, E. (2010). Fixation methods for electron microscopy of human and other liver. *World Journal of Gastroenterology*, *16*(23), 2851. doi:10.3748/wjg.v16.i23.2851

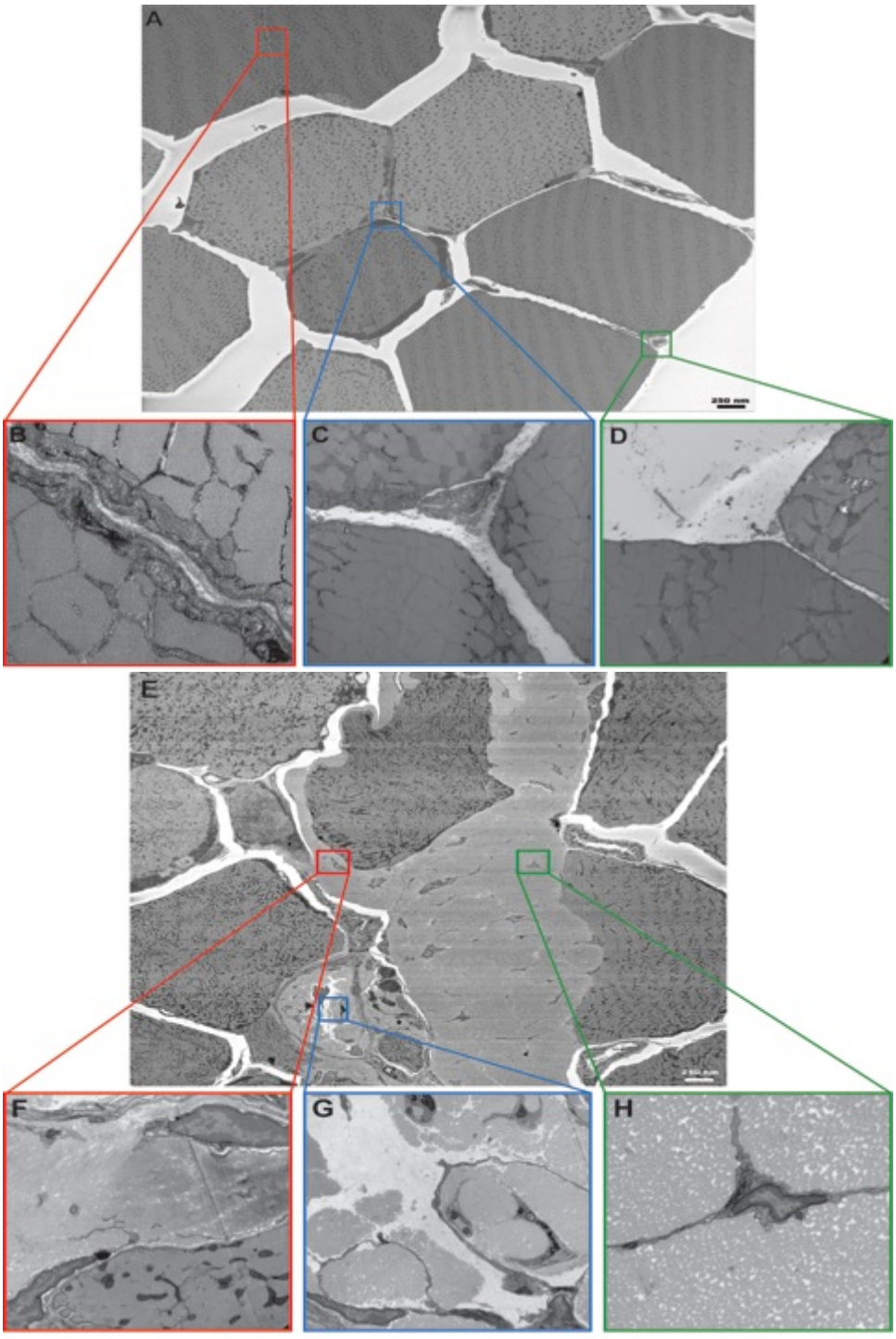

Supplemental Figure 1: **Group 1 – wildtype and double knockout mice.** A is the SEM 3View snapshot of wild-type mouse, with inlets highlighted in B-D. Inlets show representative TEM images of the boxed areas; they are not images of the actual boxed area. E-H shows similar SEM and TEM images for the double knockout mouse. SEM video and reconstruction video recordings are on file in the Mandeville Library.

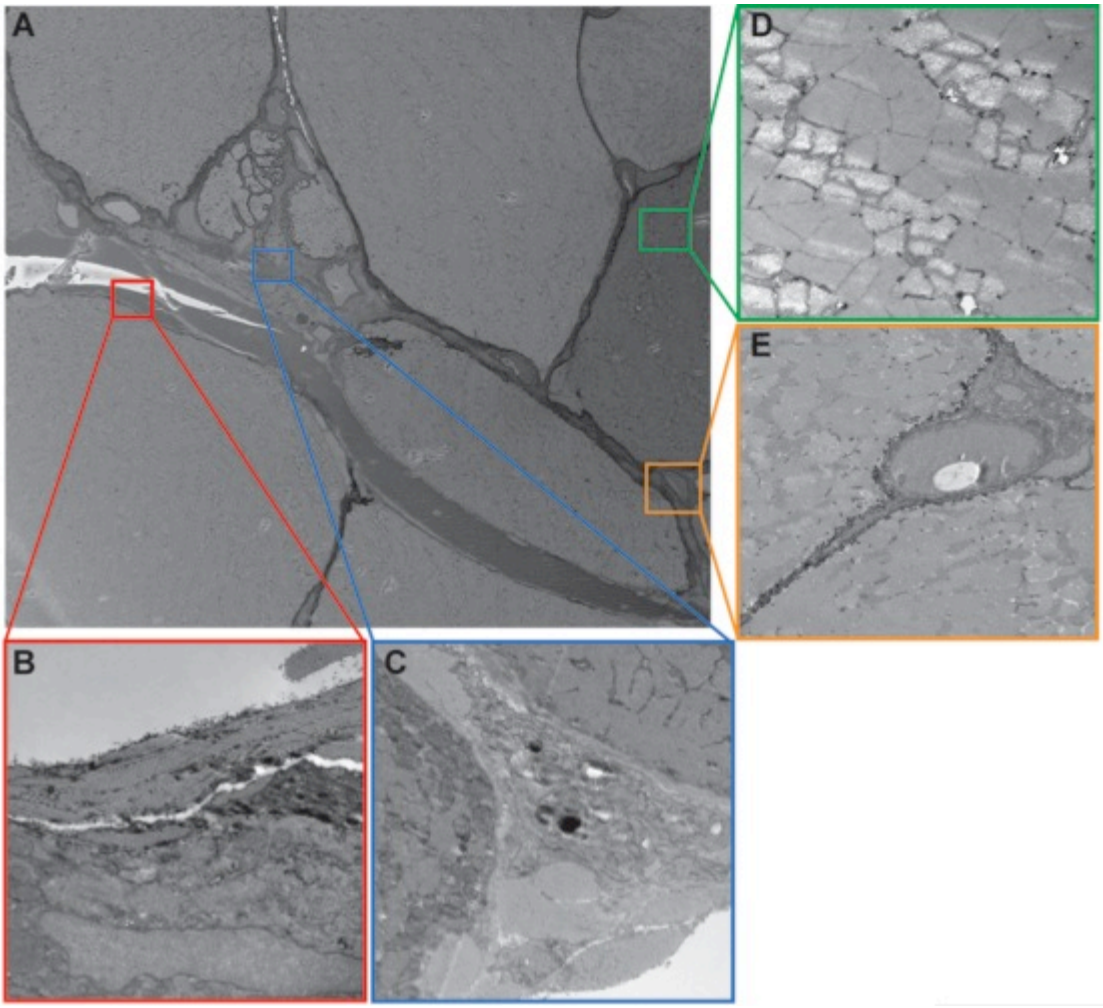

Supplemental Figure 2: **Group 2 – double knockout mouse.** A shows SEM 3View image of double knockout mouse, tibialis anterior muscle. B-E are representative TEM images found in the block face. SEM video and reconstruction video recordings are on file in the Mandeville Library.

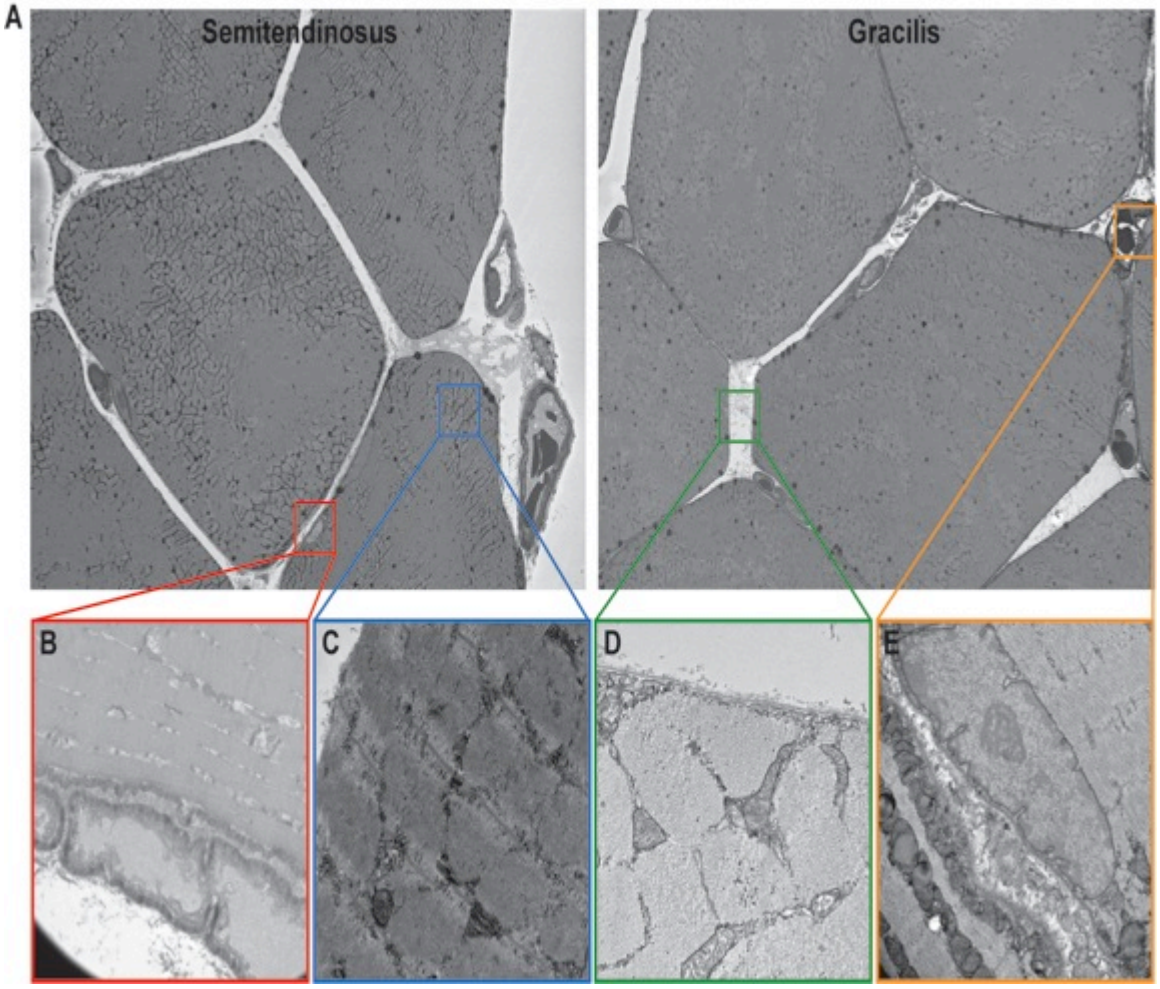

Supplemental Figure 3: **Typically developing patient.** A shows two different SEM 3View videos taken; semitendinosus muscle on the left and gracilis muscle on the right. B-E are TEM images of representative images found in areas similar to those boxed in the SEM images. SEM video and reconstruction video recordings are on file in the Mandeville Library.

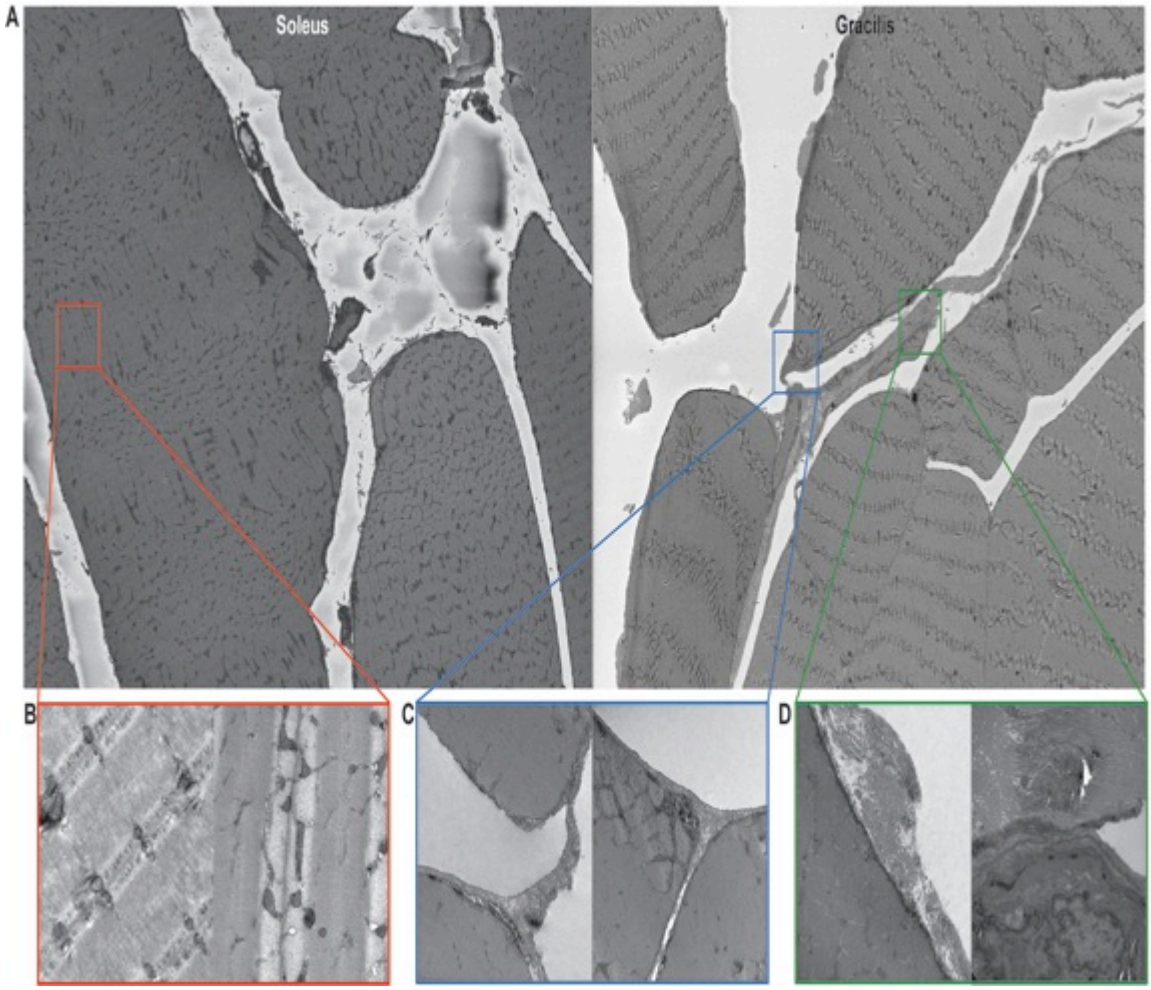

Supplemental Figure 4: **Cerebral palsy patient 1.** A shows two different SEM 3View videos taken; soleus muscle on the left and gracilis muscle on the right. B-D boxes have two TEM images of representative images found in areas similar to those boxed in the SEM images. SEM video and reconstruction video recordings are on file in the Mandeville Library.

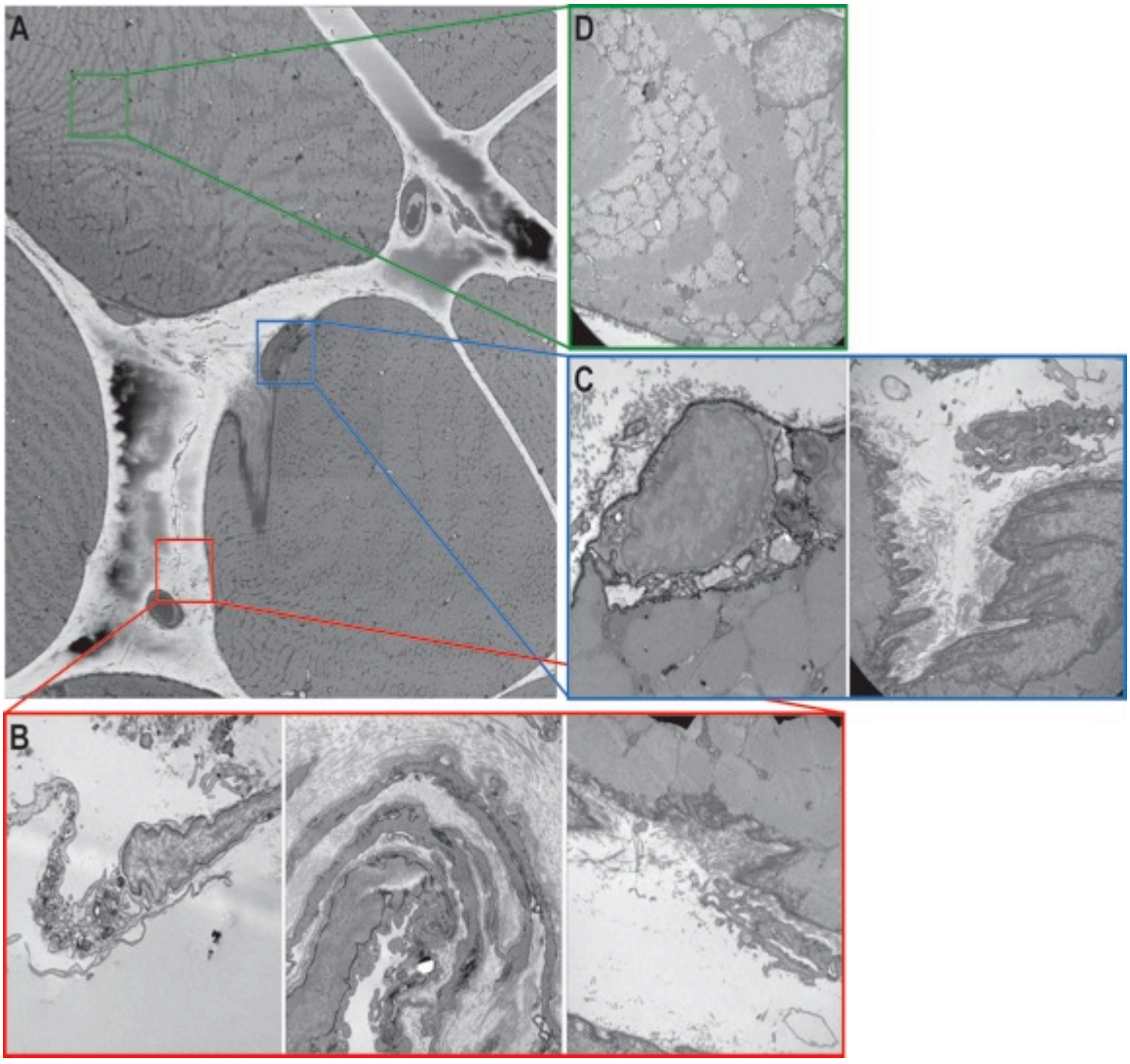

Supplemental Figure 5: **Cerebral palsy patient 2**. A is the SEM 3View image of the gastrocnemius muscle of a patient with cerebral palsy. B boxes show different fibroblasts, collagen bundles and other ECM components found around the areas surrounding myofibers. C boxes show a satellite cell and myonucleus, both of which were found in this 3View sample. D shows the dark and light A and I band patterns respectively. SEM video and reconstruction video recordings are on file in the Mandeville Library.

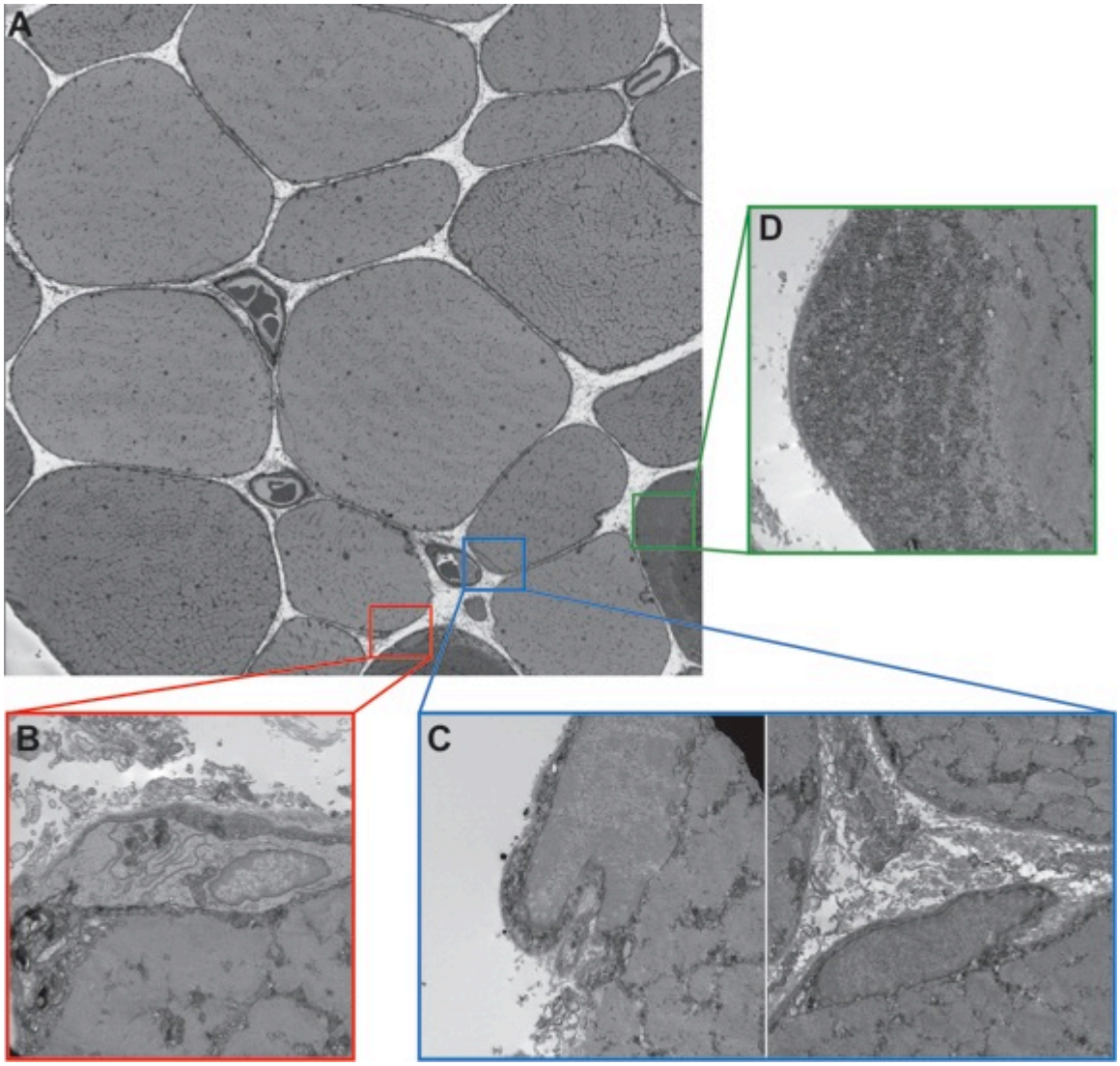

Supplemental Figure 6: Cerebral palsy patient 3. A is the SEM 3View image with B-D showing representative TEM images of areas found commonly around the sample. SEM video and reconstruction video recordings are on file in the Mandeville Library.